Exp Fluids (2013) 54:1613
DOI 10.1007/s00348-013-1613-4

RESEARCH ARTICLE

# Validity of thermally-driven small-scale ventilated filling box models

**Jamie L. Partridge · P. F. Linden**

Received: 8 May 2013 / Revised: 10 September 2013 / Accepted: 5 October 2013 / Published online: 24 October 2013


**Abstract** The majority of previous work studying building ventilation flows at laboratory scale have used saline plumes in water. The production of buoyancy forces using salinity variations in water allows dynamic similarity between the small-scale models and the full-scale flows. However, in some situations, such as including the effects of non-adiabatic boundaries, the use of a thermal plume is desirable. The efficacy of using temperature differences to produce buoyancy-driven flows representing natural ventilation of a building in a small-scale model is examined here, with comparison between previous theoretical and new, heat-based, experiments.

## 1 Introduction

Over the past 50 years, there have been many studies of the flow induced by plumes within enclosures. The canonical flow is the 'filling box' which describes the production of a stable stratification by a buoyant plume in a closed container (Baines and Turner 1969). This work was based on earlier plume theory (Morton et al. 1956). Recently, the filling box has received even more attention due to its application in naturally ventilated spaces. It has been shown that, when the enclosure was connected to the exterior by vents, steady-state configurations are possible in which the interior stratification took simplified forms and remained constant in time (Linden et al. 1990). In particular, it was shown that the stratification produced by a single plume with a constant buoyancy flux produced a two-layer stratification. The height of the interface between the layers was set by the size of the vents and was independent of the strength of the plume. This theory was validated with the use of small-scale experiments using saline, rather than thermal, plumes in water. The use of water as the working fluid and salt as the stratifying agent allowed dynamical similarity between the small-scale laboratory models and full-scale flows found in buildings (Linden 1999). Since then, this technique has been used repeatedly to analyse various different arrangements of natural ventilation flows.

Multiple plumes have been studied (Linden and Cooper 1996), and the effects of external wind forcing have been examined (Hunt and Linden 2001; Coomaraswamy and Caulfield 2011). Another important issue when considering natural ventilation flows is the timescales involved in the problem. These are key when considering scenarios where steady states may not be possible, e.g. theatres, lecture halls, etc. The approach to steady state in displacement ventilation when a steady plume source was turned on has been examined (Kaye and Hunt 2004), and the transients as the plume source strength is changed have also been studied (Bower et al. 2008).

There have been several studies of natural ventilation driven by distributed heating using a heated base and water as a working fluid (e.g. Gladstone and Woods 2001; Fitzgerald and Woods 2007). These configurations produce well-mixed interiors by high Rayleigh number convection. On the other hand, very little has been done with thermal plumes rising from small sources, which produce stable stratification in the interior space. The effects of a distributed source of buoyancy in the same boundary as a localised source have been examined (Chenvidyakarn and Woods 2008). It should be noted that in this case, the enclosure was not naturally

J. L. Partridge (✉) · P. F. Linden
DAMTP, Centre For Mathematical Sciences,
Cambridge University, Cambridge, UK
e-mail: jlp56@cam.ac.uk

ventilated, but rather the ventilation flow rate through the space was specified. The experiments compared well with a model that ignored the effects of diffusion of heat, but the dynamical similarity of the flow was not examined.

There are situations where it will be more desirable to use heat as the stratifying agent, for example when investigating the interaction between non-adiabatic (i.e. non-insulating) boundaries and the flow, which are extremely difficult to achieve using salt stratified fluid. The use of heat rather than salt has two effects: first, the buoyancy forces associated with temperature differences in water are much smaller than those achievable using salt, and second, heat has a much larger (by a factor of about 100) molecular diffusivity than salt in water. This paper describes experiments using thermal plumes in an insulated but ventilated enclosure to examine the effects of using heat as the stratifying agent. A single thermal plume with a constant buoyancy (heat) flux is located on the floor of the enclosure, and vents are located at the top and bottom of the enclosure to reproduce the displacement ventilation configuration discussed in Linden et al. (1990).

The outline of the paper is as follows. The basics of dynamic similarity are outlined in Sect. 2, where the values of Reynolds and Péclet numbers are investigated. Section 3 gives a brief review of the theory of displacement ventilation produced by a single heat source and is followed by Sect. 4 in which details of the experiments are described. Section 5 compares theoretical and experimental results and examines the effects of the larger molecular diffusivity of heat compared with salt. Finally, conclusions of the work are given in Sect. 6.

## 2 Dynamic similarity

At full scale, the ventilation flow in a building is dominated by inertia and advection and, except for regions very close to boundaries, molecular viscosity and diffusion are negligible. When the length scales of the system are reduced, viscous dissipation and conduction of heat become more significant and, in order to ensure that the same dynamical balances hold in laboratory-sized models, it is essential that inertia and advection still dominate the balance of forces. For a flow with velocity scale $U$, length scale $H$, kinematic viscosity $\nu$ and molecular diffusion coefficient $\kappa$, the balance between inertia and viscous forces is described by the Reynolds number $Re \equiv UH/\nu$ and between advective and molecular heat transfer by the Péclet number $Pe \equiv UH/\kappa$.

When the flow is driven by buoyancy forces associated with density differences $\rho_1 - \rho_2$, the velocity scales as $U \sim \sqrt{g'H}$, where the reduced gravity $g' = g\left(\frac{\rho_1-\rho_2}{\rho_2}\right)$ and $H$ the height of the enclosure, so that

$$Re \sim \frac{g'^{1/2}H^{3/2}}{\nu}$$

and

$$Pe \sim \frac{g'^{1/2}H^{3/2}}{\kappa}. \quad (1)$$

At full scale, buoyancy-driven air flows have both $Re$ and $Pe$ of order $10^5$. Using water as the working fluid (with smaller values of $\nu$ and $\kappa$) and producing large density differences associated with salinity variations makes it possible, even in small-scale models where $H$ is reduced significantly, to achieve values of $Re \sim 10^4$ and $Pe \sim 10^6$. These laboratory values are comparable to full-scale values and large enough to be confident that the same dynamical balances hold at the laboratory scale (Linden 1999).[1]

The use of heat (in water) to provide the buoyancy forces has two effects. The first is that the density differences achievable are smaller than those that can be obtained with salt: the maximum value of $g'$ is approximately 3 cm s$^{-2}$ for heat compared with about 30 cm s$^{-2}$ for salt, which reduces maximum velocities (and $Re$) by a factor of about 3. Second, the thermal diffusivity of heat (in water) is approximately 100 times greater than that of salt and the values of $Pe$ are reduced by two orders of magnitude, and so conduction of heat may be expected to play a larger role at the laboratory scale.

## 3 Emptying the filling box

We consider displacement ventilation driven by a single plume in an enclosure. The enclosure has openings at the top and bottom, and the flow is driven by a point source located on the floor, which provides a constant buoyancy flux $B$. The configuration differs from that used in earlier theory, in that the openings are located on the sides of the enclosure rather than in the top and bottom boundaries (Fig. 1) (Linden et al. 1990). Because of this, the original theory is slightly adjusted by defining vertical distances relative to the mid-heights of the (equal height) top and bottom openings as defined in Fig. 1.

Heat from the plume accumulates in an upper layer and drives warm fluid out through the upper openings, and there is a consequent flow of cool ambient fluid in through the lower openings. The ventilation flow rate $Q_v$ is driven by the hydrostatic pressure associated with the warm upper layer

[1] Strictly speaking, if we are considering flow at smaller scales within the model building such as through an opening, then both the full-scale and laboratory scale values are reduced by a factor of up to 10.

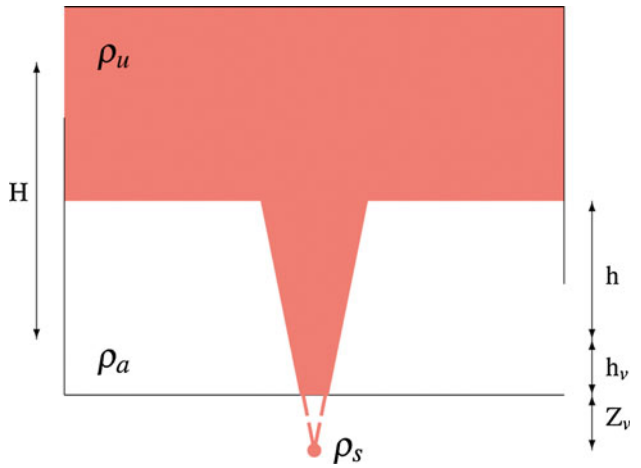


**Fig. 1** Schematic of the enclosure and the heat source. $H$ is the vertical separation between the middle of the openings, which are each of (equal) height $2h_v$, $h$ is the distance above the middle of the lower opening to the density interface, and $Z_v$ is the distance from the source to the virtual origin. The upper layer, ambient and plume supply densities are labelled $\rho_u$, $\rho_a$ and $\rho_s$, respectively

$$Q_v = A^* \sqrt{g'(H-h)}, \tag{2}$$

where $g' = g(\rho_a - \rho_u)/\rho_a$, $\rho_a$ is the density of the ambient fluid that occupies the lower layer and $\rho_u$ is the density of the warm upper layer. The 'effective opening area' $A^*$ is a combination of the upper and lower opening areas, $a_t$ and $a_b$, respectively, and is given by

$$A^* = \sqrt{\frac{(2c_b c_t a_b^2 a_t^2)}{(c_b a_b^2 + c_t a_t^2)}}, \tag{3}$$

where $c_t$ and $c_b$ are loss coefficients associated with flow through the upper and lower openings (Linden et al. 1990).

In steady state, $Q_v$ and $g'_u$ are equal to the volume flux $Q_p$ and buoyancy $g'_p$ of the plume at the interface height, which can be found from classical plume theory

$$Q_p = CB^{1/3}\tilde{h}^{5/3}$$

and

$$g'_p = C^{-1}B^{2/3}\tilde{h}^{-5/3}, \tag{4}$$

where $\tilde{h}$ is the distance of the interface above the virtual origin of the plume and $C \sim 0.2$ is a constant which parameterises the inflow of ambient fluid into the plume (Morton et al. 1956).

In both the saline and thermal experiments, the plume is established by providing a small flow rate $Q_s$ of buoyant fluid through the source. In order to represent this in terms of a pure unforced plume, we include a virtual origin $Z_v$, which extrapolates the plume back to an idealised point source (see Fig. 1). Following Woods et al. (2003), the virtual origin is calculated by matching the known volume flux at the source

$$Q_s = CB^{1/3}Z_v^{5/3}, \tag{5}$$

and solving for $Z_v$.

Matching the volume flux and buoyancy of the upper layer with that of the plume at the height of the interface $\tilde{h} = h + h_v + Z_v$ we obtain:

$$\frac{A^*}{C^{3/2}H^2} = \sqrt{\frac{(\zeta+\zeta_v)^5}{(1-\zeta)}}, \tag{6}$$

where the dimensionless interface height and virtual origin location are given by

$$\zeta = \frac{h}{H} \quad \text{and} \quad \zeta_v = \frac{(h_v + Z_v)}{H}. \tag{7}$$

Equations (6) and (7) determine the steady-state interface height $h$, which can then be related back to the height from the base of the tank by adding $h_v$.

The steady-state upper layer temperature is determined by equating the reduced gravity $g'_u$ of the upper layer to the reduced gravity of the plume at the interface height,

$$g'_u = g'(h + h_v + Z_v) = C^{-1}B^{2/3}(h + h_v + Z_v)^{-5/3}, \tag{8}$$

or noting that

$$g'_s = g\left(\frac{\rho_a - \rho_s}{\rho_a}\right) = C^{-1}B^{2/3}Z_v^{-5/3}, \tag{9}$$

where $g'_s$ is the reduced gravity of the plume at the source. Hence,

$$g'_u = g'_s Z_v^{5/3}(h + h_v + Z_v)^{-5/3}. \tag{10}$$

Additionally, heat losses through the fabric of the enclosure will reduce the reduced gravity of the upper layer. This can be represented as an additional buoyancy loss of the upper layer $B_l$, which, in steady state, results in the following buoyancy balance

$$B_l + B_u = B, \tag{11}$$

where $B_u$ is the buoyancy flux out of the upper layer. Equating this in terms of reduced gravities and flow rates of the enclosure, we obtain

$$\frac{g'_u \mathbf{U} A}{\rho C_p} + g'_u Q_v = B, \tag{12}$$

which can then be solved for the reduced gravity of the upper layer

$$g'_u = \frac{\rho C_p B}{\mathbf{U}A + \rho C_p C B^{1/3}(\zeta+\zeta_v)^{5/3}H^{5/3}}, \tag{13}$$

where the $\mathbf{U}$ value of the enclosure, a measure of insulation, was obtained from heat loss experiments and

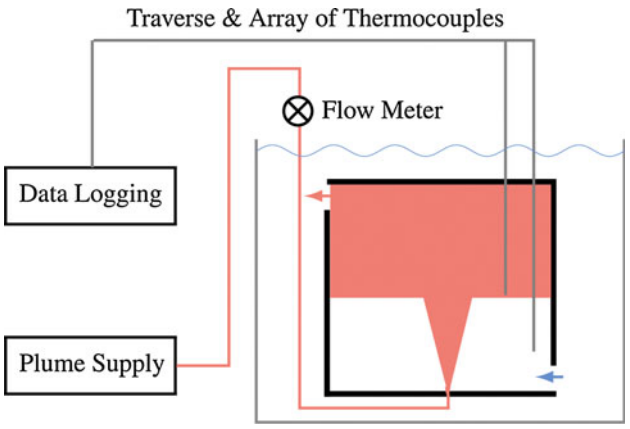


**Fig. 2** Schematic of the experimental setup showing the enclosure, with vents represented as gaps in the sides, immersed in a larger 'environmental' tank

is detailed in Sect. "Appendix 1". $A$ is the area in contact with the upper layer, which in terms of the width $L_1$ and depth $L_2$ of the enclosure, is defined as

$$A = 2(H + 2h_v)(1 - (\zeta + h_v))(L_1 + L_2) + L_1 L_2. \quad (14)$$

## 4 Experiments

The experimental tank (Fig. 2) is highly adjustable and constructed with boundaries that can be changed between insulating and non-insulating. In 'adiabatic mode', the six sides of the tank are made from acrylic sheeting with an air gap sandwiched between them, producing a 'double-glazed' insulating boundary. To provide heat transfer to the enclosure, the inner sheet of four of these sides can be replaced with brass plates with custom-built heater mats attached to the rear. This gives full control over the boundary conditions, including the ability to have time varying heat fluxes, over the floor, ceiling and two of the sides. Dimensions of the tank are shown in Fig. 3.

The plume was supplied from a 1 kW heater bath with a built-in pump. The flow rate from the pump was controlled via a valve and monitored using an in-line flow meter. This hot water supply is then linked up to a special plume nozzle [2] to ensure the plume is turbulent directly above the source. The temperature of the supply was monitored via a T-type thermocouple just below the nozzle. This was done for two reasons: first, to be able to record the supply temperature, as there were losses from the heater bath to the source and second, to monitor the supply temperature to check that it remained constant throughout the experimental run. The hot water bath itself was resupplied by a simple gravity feed from the large ambient reservoir. This method of establishing a plume was chosen over the alternative of an electrically heated element as the power density of such an element would result in localised boiling at the source.

The parameters of the experiments conducted are summarised in Table 1. The parameters were chosen to ensure that the flow from the plume was turbulent and predominantly buoyancy driven within the enclosure.

The influence of source conditions of the plume is determined by the size of $Z_v$, the virtual origin. For the experimental runs 1–10, the mean of $Z_v$ was 2.77 cm with standard deviation 0.03 cm, and for runs 11–17, the mean $Z_v$ was 2.15 cm with standard deviation 0.02 cm. Given the small variation, the average value was used in each case.

The temperatures, and hence the reduced gravities, of the interior of the filling box were monitored in two ways using T-type thermocouples. The first was via an array of eight, equally spaced, thermocouples extending over the height of the tank. The second method was a traversing thermocouple that travelled the height of the tank. These arrangements allowed temperatures to be recorded at different fixed heights throughout the experiments and for temperature profiles to be measured over the full vertical extent of the enclosure. It is possible, given the location of the measurement apparatus, that there could be some leakage of fluid where the instruments enter the enclosure. However, as the apparatus was always located within the enclosure, and their entrance contained a rubber seal, no leakage of buoyant fluid was ever observed.

The thermocouples were calibrated in LabView by placing them in a water bath over an appropriate temperature range (10–80 °C). With careful calibration, accuracies to within ±0.1 °C were obtained. Temperatures were recorded using National Instruments equipment. The array was recorded using NI-9213, capable of recording from 16 thermocouples at 5 Hz, and data were logged using LabView SignalExpress. The traverse mechanism itself was driven via a NI-6008 controller, to send pulses to a stepper motor, which was also controlled via LabView. The stepper motor was pulsed at 125 Hz and took approximately 3 min to traverse 28 cm through the tank. This traverse speed was chosen to minimise the lag associated with the thermocouple, reducing the speed of the stepper motor further made no difference to the temperature profile recorded.

The loss coefficients, $c_t$ and $c_b$, were both assigned the value 0.6 to represent losses as the flow passes through the sharp openings. These loss coefficients have been previously shown to be dependent on the buoyancy difference between the fluid in the enclosure and the ambient fluid (Holford and Hunt 2001). However, calibration experiments were carried out for the current setup, and no dependence was seen, rendering a constant value suitable. This insensitivity is due to the relatively small buoyancy

[2] Originally designed by Paul Cooper, see figure 6 of Hunt and Linden (2001).

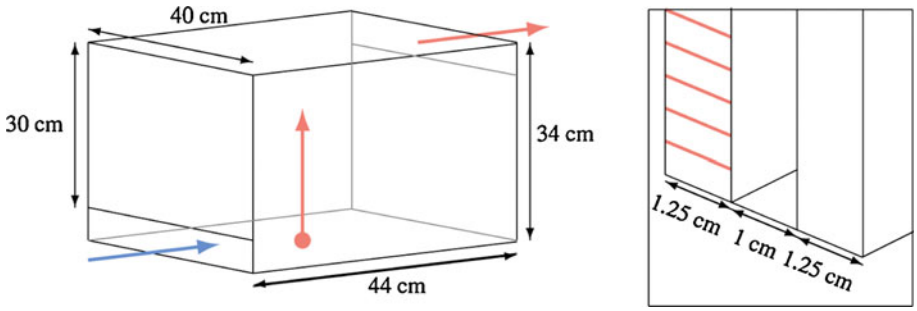


**Fig. 3** Diagram of the enclosure used in the experiments. The exploded view shows the composite construction of the sides of the tank, the *dashed region* indicates the inner section, which can be changed on four of the six boundaries to allow for heat transfer

**Table 1** Table of experimental parameters

| Run | $\Delta T_s$°C | $Q_s$ cm$^3$ s$^{-1}$ | Lower opening area $a_b$ cm$^2$ | Upper opening area $a_t$ cm$^2$ |
|---|---|---|---|---|
| 1–10 | 10.22–12.04 | 2.2 | 160 | 10–140 |
| 11–17 | 16.83–19.14 | 1.5 | 160 | 10–100 |

differences associated with these thermal plume experiments compared to those driven by salinity.

Due to the experimental setup, the heater bath supplying the plume also fluctuated throughout the experiment. Typically, the plume supply temperature had a variation of 1 %, which resulted in negligible fluctuations in the buoyancy flux of the plume, and a constant value was taken. In addition, there will be losses through the fabric of the enclosure. This could be included theoretically using Eq. (13) but is neglected as, for the experiments considered here, the heat loss through the fabric was $\sim 1\%$ the heat flux of the plume.

## 5 Results

A visualisation of an experiment, recorded using DigiFlow, is shown in Fig. 4. Initially, as in Fig. 4a, the tank is filled with ambient fluid before the turbulent plume is introduced, which rises towards the top of the enclosure and entrains ambient fluid as it does so. Figure 4b–c shows the plume impinging on this boundary and spreading radially as a gravity current before hitting the walls of the enclosure inducing further mixing into the interior. As this occurs, light fluid begins to exit via the upper opening and ambient fluid enters via the lower opening. After the initial transient, and the mixing at the side walls diminishes, a well-mixed upper layer forms. The interface is not perfectly horizontal during this transient stage, as the mixing in the upper layer driven by the plume causes interfacial waves. The amplitude of these interfacial waves decreases as the experiment settles into the steady state of the system, as displayed in Fig. 4d. However, it is worth noting that large amplitude waves can persist if the velocity of the inlet fluid is large. This can be minimised in experiments by making sure that the lower opening is at least twice the size of the upper opening. Any waves that do continue to propagate on the interface, even in steady state, are oscillatory in time and so measurements are not biased by their location.

Figure 5 shows the temperature data from the fixed thermocouples during the transient stage. In this figure, time $t$ has been normalised with a timescale for filling an unventilated box with a plume of strength $B$, known as the filling-box timescale

$$T_f = \frac{S}{CB^{1/3}H^{2/3}}, \tag{15}$$

where $S$ is the floor area. As expected, the lower layer stays at ambient temperature throughout the experiment, although the fluid in this region is constantly being exchanged for fresh fluid from the inlet and being extracted out of the lower layer via entrainment in the plume. Initially the upper layer increases in temperature rapidly before approaching the final steady-state temperature of the system. In the final steady state, i.e. for $\frac{t}{T_f} > 4$ here, there are two well-mixed layers, as seen in the visualisation of Fig. 4d, with one thermocouple sitting somewhere on the interface. Consequently, this thermocouple has a midrange temperature, and fluctuations, produced by the interfacial waves, are visible.

A typical temperature profile of an experiment is shown in Fig. 6. The profile shows two relatively well-mixed layers separated by an interface of finite thickness. The small-scale fluctuations are noise from the thermocouple readings. The apparent asymmetry in the interface is an artefact of the traversing procedure, from top to bottom, and induced by the lag in the thermocouples readings. This has been confirmed by comparing data between the traversed and fixed thermocouples. The finite thickness of the interface leads to some ambiguity in the definition of the lower layer height $h$. For definiteness, $h$ is defined as the height at which the temperature is the mean of the upper and lower layer temperatures, calculated in the regions where the vertical temperature gradient is less than 0.01 needs units. The width $L$ of the interface is then defined by extrapolating the vertical temperature gradient

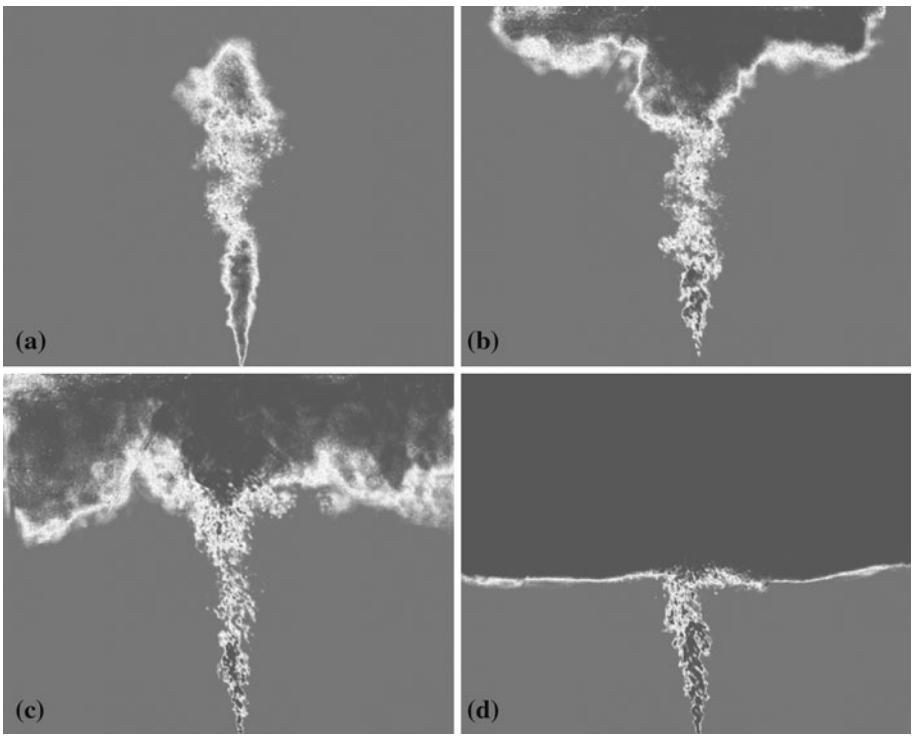


**Fig. 4** A series of images from an experiment where the buoyant plume fluid was dyed to aid visualisation. The initial rise of the plume is shown in **a–c** show the impact of the fluid on the ceiling and its subsequent descent into the enclosure, and **d** the final steady state with two uniform layers separated by a density interface

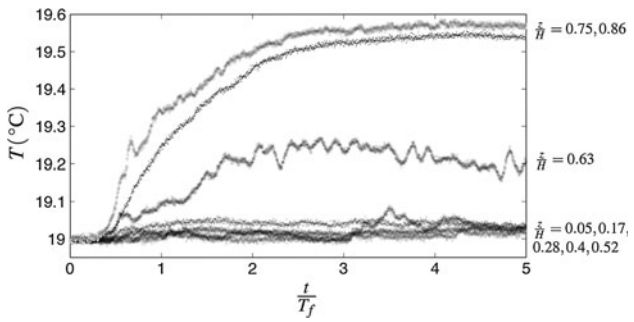


**Fig. 5** Temperature data from the fixed thermocouples with $\frac{A^*}{H^2} = 0.0734$, plotted against the dimensionless time $\frac{t}{T_f}$. The labels give the height of the thermocouples. In this case, the thermocouple at $z/H = 0.63$ is located in the interface between the two layers

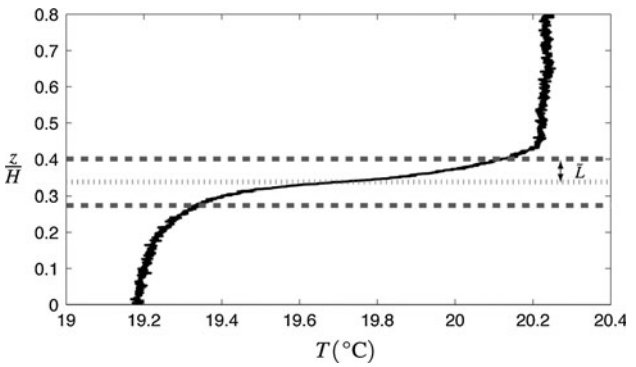


**Fig. 6** A typical temperature profile of steady state, with $\frac{A^*}{H^2} = 0.0186$, showing interface thickness $L$. The height $\zeta$ is determined by the location of the temperature mid way between that of the two layers

at $z = h$ and extending it as a straight line until it intersects the mean temperature of the two layers.

Figure 7 shows measurements of the steady-state interface height $h/H$ plotted against the effective area $A^*$ of the openings. The interface rises with increasing $A^*$ due to the increased flow through the enclosure which needs to be balanced by an equal volume flux in the plume, which, in turn, increases as $\sim z^{5/3}$. The solid curve is the result of the theoretical prediction (6), and the results compare very well with the model and those given in figure 12 of Linden et al. (1990) for the interface height location for a salt plume. Due to the ambiguity in defining the interface height, the error bars are the width of the interface region in each experiment.

Corresponding to this rise in interface height with increasing $A,^*$ the temperature of the upper layer decreases, since the temperature of the plume decreases as $\sim z^{-5/3}$. Results and comparison with the theoretical predictions are shown in Fig. 8.

The smaller values of $Pe$ mean that diffusion of heat in the interior of the flow is more important than for saline experiments. This effect is largest in regions of high temperature gradients, i.e. at the interface between the upper and lower layers. Kaye et al. (2010) examined this effect by proposing a balance between diffusion, acting to smear the interface, and entrainment in the plume, which acts to sharpen the interface. Considering a simple one-dimensional model of a diffusive layer between an initial jump in density,

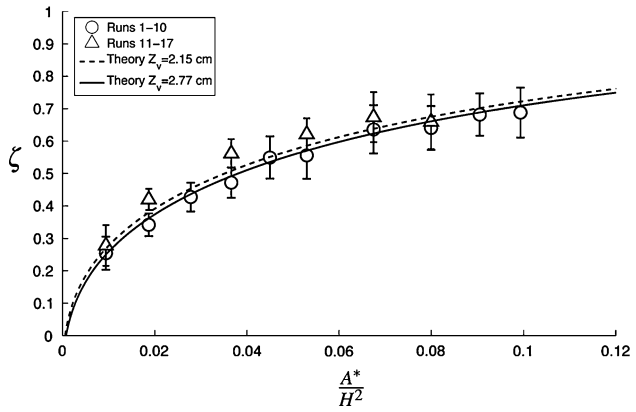


**Fig. 7** The steady-state interface height plotted against the effective area of the openings. The *curves* correspond to (3.5) with $C \sim 0.2$ and different values of the virtual origin. The *error bars* correspond to the width $L$ of the interface

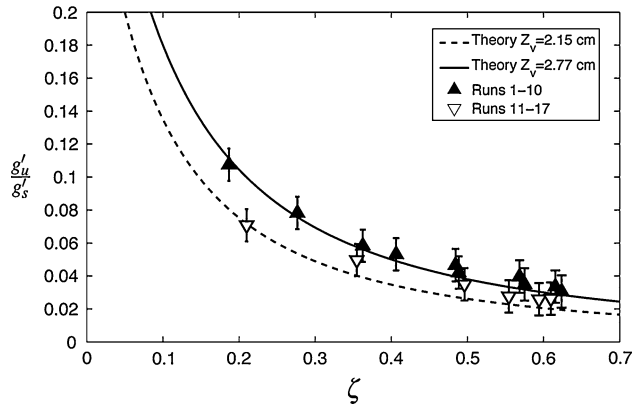


**Fig. 8** Steady-state upper layer temperature: theoretical results with experimental data plotted for comparison

i.e. a perfectly sharp interface, the standard solution is that of a complimentary error function,

$$T(z,t) = \frac{T_0}{2}\left(1 + \mathrm{erf}\left[\frac{z}{(4\kappa t)^{1/2}}\right]\right), \tag{16}$$

with $t$ time, $z$ the location in the profile, $\kappa$ the thermal diffusion coefficient and $T_0$ the initial temperature step. This solution is used to define a diffusive length scale and hence growth rate of the diffusive layer

$$\frac{L}{2} \sim (4\kappa t)^{1/2}, \tag{17}$$

where $L$ is the total interface thickness. This interfacial region then grows in volume as

$$Q_{\mathrm{int}} = S\frac{\mathrm{d}L}{\mathrm{d}t} = \frac{8\kappa S}{L}, \tag{18}$$

where $Q_{\mathrm{int}}$ is the effective volume flow rate into the interface. In a steady state, this growth in the interface is balanced by entrainment into the plume across the interfacial layer

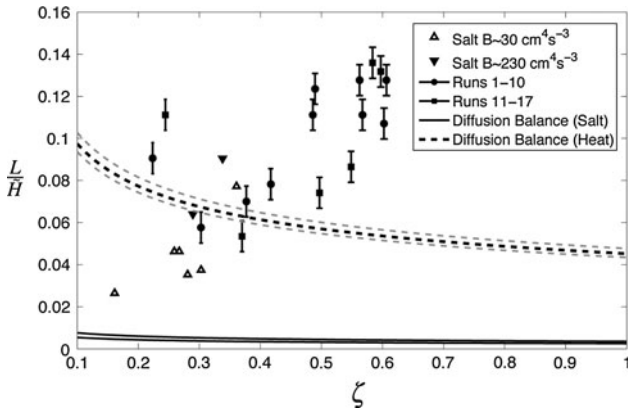


**Fig. 9** Interface width with varying interface height. The interface widths shown here correspond to the *error bars* of Fig. 7. Data are shown from both salt and temperature based experiments. The diffusion balance model is also included for each case with the upper and lower theoretical curves representing the range of $B$ used within the experiments

$$\frac{8\kappa S}{L} = CB^{1/3}\left[\left(h + Z_v + \frac{L}{2}\right)^{5/3} - \left(h + Z_v - \frac{L}{2}\right)^{5/3}\right], \tag{19}$$

where the right-hand side is the change in volume flux in the plume as it rises from the bottom to the top of the interface.

Figure 9 shows the normalised interface thickness, with $\tilde{H} = H + 2h_v$ being the total height of the enclosure, plotted against the interface height. As previously stated, the interfacial thickness was determined by fitting a straight line to the traversed probe data in the region of mean density of the layers to overcome any lag associated with the probe. Dye concentrations were also examined, see Cenedese and Dalziel (1998) for technical details and Sect. "Appendix 2" for comparison, and show good agreement with the interfacial thicknesses found using the best fit line. Data are shown from the experiments discussed in this paper along with salt-based experiments and suggest a positive trend between the interface thickness and interface location. This trend is the opposite to that expected from the balance given in (19), which predicts $L \sim h^{-1/3}$ for $L << h$. This predicted thinning of the interface with increasing $h$ results from increased entrainment into the plume with increasing height. The experiments conducted appear to show that the interface thickening is not diffusion controlled and is not a result of using a thermal plume.

## 6 Conclusion

We have investigated the validity of using thermal plumes in the filling box context, and seen that there is good

agreement with the non-diffusive, inviscid theory presented in earlier work. This is despite the fact that the Reynolds and Péclet numbers are not at their respective full-scale values. This agreement enables a thermal plume to be used reliably in place of a saline plume and will allow subsequent work, where the boundaries of the enclosure are made non-adiabatic, to be carried out with confidence.

The observed interface thickness is larger and has opposite dependence on the interface height than predicted by including the effects of increased molecular diffusion within the space. The reasons for these discrepancies are unclear. As shown in Figs. 4 and 5, the interface is not planar nor stationary, but supports internal and interfacial waves generated by the plume and by the flow in the layers above and below. It is possible that wave breaking may be a cause of the thickening of the interface as its stability decreases with $h$, consistent with the data in Fig. 9. The data does suggest that the increased interfacial thickness is not a result of increased diffusion in the interior, i.e. not a consequence of using a thermal plume.

**Acknowledgments** This project is the subject of an Industrial CASE PhD Studentship, which was awarded by the Knowledge Transfer Network for Industrial Mathematics, and is funded by the UK Engineering and Physical Sciences Research Council and by ARUP [EP/I501290/1]. We would also like to thank Dr Jake Hacker of ARUP, Dr Stuart Dalziel for his help in the laboratory and the technicians at DAMTP: David Page-Croft, Colin Hitch and John Milton.



## Appendix 1: Heat loss

Even though the tank has been set up to be well insulating there is still heat loss, although given the design it should be minimal. To get an estimate of the heat loss, experiments were conducted.

### Experimental calculation

To determine the heat loss experimentally, the tank was initially filled with hot fluid, the vents sealed and left to cool in the larger ambient container. A stirrer was located inside the tank to provide some gentle mixing to keep the interior well mixed and of uniform temperature. The temperature inside and outside of the tank was recorded using T-type thermocouples. The thermocouples inside the enclosure verified that the interior remained well mixed by the stirrer.

Given these temperature data, we can calculate an experimental $U$-value of the container, which can then be used in the relation

$$\mathscr{H}_{\text{loss}} = \mathbf{U}\hat{S}\Delta T \tag{20}$$

to determine the heat loss. $\hat{S}$ is the surface area of the inside of the box and $\Delta T$ is the temperature difference between the interior and the ambient, formally $\Delta T = T_{\text{i}} - T_{\text{a}}$. To calculate this experimental $U$-value, Newton's law of cooling (Incropera et al. 2010) was used

$$\theta = \exp(-\alpha t), \tag{21}$$

where $\theta = \frac{(T-T_{\text{a}})}{(T_0-T_{\text{a}})}$ is the non-dimensional temperature, $\alpha = \frac{\hat{S}\mathbf{U}}{(mc_p)}$, $m$ the mass of fluid and $c_p$ the specific heat capacity. The validity of this approach is ensured by keeping the interior of the tank well mixed with the stirrer. This effectively makes sure that the relevant Biot number

$$Bi = \frac{hL}{k}, \tag{22}$$

where $h$ is the convective heat transfer coefficient, $L$ a typical length scale and $k$ the thermal conductivity, is small.

Given the experimental setup, the stirrer itself will be adding some heat into the system. The power of the stirrer was given as 7 W and so an approximation to the $U$-value for the container was found by fitting a line to the temperature data. This allowed the $U$-value of the total system (i.e. including the heat gain from the stirrer) to be calculated using (21). This can then be used in (20) to determine the heat loss, which can then be corrected by adding the power of the stirrer. This equation can then be inverted to solve for the U-value. Doing this, we find a $U$-value of 5.50 $\text{Wm}^{-2}\ \text{K}^{-1}$ for the container. This newly derived $U$-value was reinserted into Eq. (20) to obtain the heat loss of the system during a typical experiment (Fig. 10).

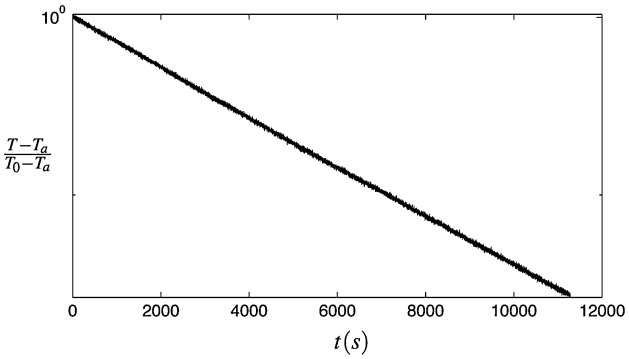


**Fig. 10** Heat loss calibration: time series showing the temperature evolution inside the enclosure

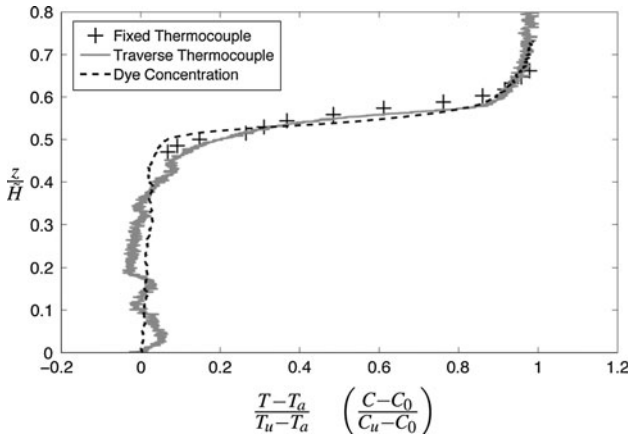


**Fig. 11** Dye concentration comparison: Temperature-based experiments. Where $C$ is the dye concentration

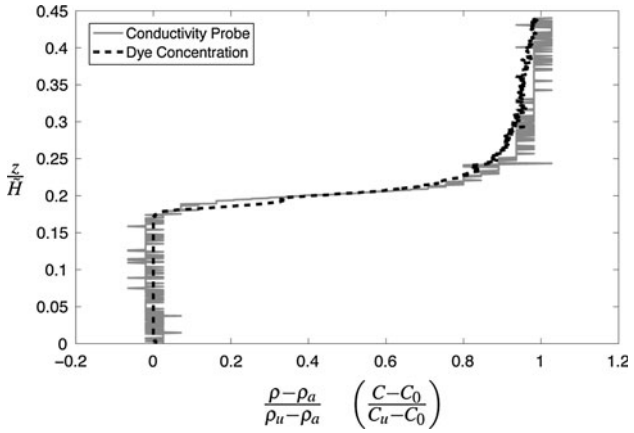


**Fig. 12** Dye concentration comparison: Salt-based experiments

If the heat loss from the container is examined using Eq. (20) with $S$ as the surface area of the inside of the enclosure in contact with the upper layer and a typical temperature difference of 1 °C, we get a heat loss value of $\sim$1.5 W. Typically, the plume will have a heat flux of $\sim$100 W and so the heat loss is comparatively small.

## Appendix 2: Dye concentration comparison

Figures 11 and 12 show the comparison between dye concentration data, using dye attenuation (Cenedese and Dalziel 1998), and the traversed data for each case. Figure 11 also shows data from fixed thermocouples acquired by holding the traversing thermocouple at fixed heights.

## References

Baines WD, Turner JS (1969) Turbulent buoyant convection from a source in a confined region. J Fluid Mech 37:51–80

Bower DJ, Caulfield CP, Fitzgerald SD, Woods AW (2008) Transient ventilation dynamics following a change in strength of a point source of heat. J Fluid Mech 614:15–37

Cenedese C, Dalziel SB (1998) Concentration and depth field determined by the light transmitted through a dyed solution. In: Proceedings of the eighth international symposium on flow visualization. Paper 061

Chenvidyakarn T, Woods AW (2008) On underfloor air-conditioning of a room containing a distributed heat source and a localised heat source. Energy Build 40:1220–1227

Coomaraswamy IA, Caulfield CP (2011) Time-dependent ventilation flows driven by opposing wind and buoyancy. J Fluid Mech 672: 33–59

Fitzgerald SD, Woods AW (2007) Transient natural ventilation of a room with a distributed heat source. J Fluid Mech 591:21–42

Gladstone C, Woods AW (2001) On buoyancy-driven natural ventilation of a room with a heated floor. J Fluid Mech 441:293–314

Holford JM, Hunt GR (2001) The dependence of the discharge coefficient on density contrast. In: 14th Australasian fluid mechanics conference, pp 123–126

Hunt GR, Linden PF (2001) Steady-state flows in an enclosure ventilated by buoyancy forces assisted by wind. J Fluid Mech 426:355–386

Incropera FP, DeWitt DP, Bergman TL, Lavine AS (2010) Fundamentals of heat and mass transfer (6th edn). Wiley, New York

Kaye NB, Hunt GR (2004) Time-dependent flows in an emptying filling box. J Fluid Mech 520:135–156

Kaye N, Flynn M, Cook M, Ji Y (2010) The role of diffusion on the interface thickness in a ventilated filling box. J Fluid Mech 652:195–205

Linden PF (1999) The fluid mechanics of natural ventilation. Annu Rev Fluid Mech 31:201–238

Linden PF, Cooper P (1996) Multiple sources of buoyancy in a naturally ventilated enclosure. J Fluid Mech 311:177–192

Linden PF, Lane-Serff G, Smeed D (1990) Emptying filling boxes: the fluid mechanics of natural ventilation. J Fluid Mech 212: 309–335

Morton BR, Taylor GI, Turner JS (1956) Turbulent gravitational convection from maintained and instantaneous sources. Proc R Soc 234:1–23

Woods AW, Caulfield CP, Phillips JC (2003) Blocked natural ventilation: the effect of a source mass flux. J Fluid Mech 495:119–133